Applied Water Science (2020) 10:54
https://doi.org/10.1007/s13201-019-1119-1

ORIGINAL ARTICLE

Fabrication of Zr-doped SnO_2 nanoparticles with synergistic influence for improved visible-light photocatalytic action and antibacterial performance

Ameer Baig Ali Baig[1] · Vadamalar Rathinam[1] · Jayanthi Palaninathan[1]

Received: 4 November 2019 / Accepted: 10 December 2019 / Published online: 10 January 2020

Abstract

Zr-doped SnO_2 (Zr:SnO_2) nanostructures (NSs) were produced by simplistic and low-cost co-precipitation route. The FTIR spectra of bands on 523 and 583 cm^{-1} were witnessed though indorsed as the features of (Sn–OH) term which approves the incident of Sn–O in the synthesized samples. The Zr:SnO_2 NSs were spherical-like and composed of numerous agglomerated particles. The decreased crystallite sizes of the pristine and Zr-doped SnO_2 NPs were 41.9, 38.9 and 35.8 nm individually. Moreover, the achievable growth manner of acquired samples was deliberated through the source of the customs of nucleation and crystal growth. The photocatalytic performances of 4% of Zr-doped SnO_2 nanoparticles (NPs) were thoroughly explored in the photodegradation of methyl orange (MO) dye, thus revealing higher photocatalytic activity in the degradation of MO than pristine and 2% of Zr-doped SnO_2 under via visible-light exposure. Related to pristine SnO_2, the 4% Zr-doped SnO_2 NPs are accessible to greater photocatalytic capability, which could be essentially accredited to existing in the nominal defects of oxygen vacancies by the produced NPs. Eventually, founded on the self-assembly progression the possible development of photocatalytic mechanism was projected by means of reactive species in trapping tests as well. Also, the antibacterial action was attained against *E. coli* and *S. aureus* bacteria through agar well diffusion system.

Keywords Zr-doped SnO_2 · Nanoparticles · Photocatalytic performance · Methyl orange dye · Visible-light exposure

Introduction

Currently, the synthesis progression, reform and applications of semiconductive nanomaterials (NMs) by appropriate modules and architectural assemblies have become an investigation emphasis in numerous fields as the enlargement of nanoscience expertise and semiconductor proficiency (Hu et al. 2014). As one of the supreme prevalent metal oxide (*n*-type) semiconductors (SCs), tin oxide (SnO_2) nanostructure with the optical bandgap of ~ 3.6 eV has attracted great interests these years (Chen et al. 2019). SnO_2 nanostructured ingredients own countless distinctive optical, electrical and electrochemical properties (Bhuvaneswari et al. 2018a; Song et al. 2019), which create it favourable solid material for innumerable new applications (dye base solar cells, magnetic devices, gas sensors, optoelectronic devices, catalysts and electrode materials) including photocatalytic explore for their great photosensitivity and chemical steadiness. It is substance underscoring that SnO_2 NMs have greatly advanced electron mobility than TiO_2, while expressly constructive to the aforementioned applications (Arnold et al. 2003; Hendry et al. 2006). Nonetheless, the low quantum yield of SnO_2 quiet occurs and confines its concrete application, which is mostly owing to the firm recombination rate of photoexcited charges and the squat solar energy transformation efficacy (Fu et al. 2019). Thus it is exterme concern to increase the seperation of photo-excited charges (electron/hole) and auxiliary improve the photocatalytic properties of as-obtained SnO_2 nanomaterials. The amendment of SnO_2 with metal ions, additional SCs or else noble metals could be moderately operative to hasten the separation efficacy of photoexcited (e^-/h^+), and thus, it enriches the photocatalytic assets (Vignesh et al. 2013).

Zirconium is a precise, strong, flexible, ductile transition metal ion consuming chemical and physical belongings to

✉ Ameer Baig Ali Baig
ameerramphysics@gmail.com

[1] PG and Research Department of Physics, Muthurangam Government Arts College (Autonomous), Vellore, Tamil Nadu 632 002, India

titanium nanomaterials (NMs). It is exceedingly resistant to warmth and oxidization and is used in steel alloys as a hardening mediator and also used to sort surgical appliances. Zr^{4+} ion takes the ionic radius of 0.74 Å which is slighter than that of Sn^{2+} (0.93 Å) ion (Manjula and Selvan 2017). While SnO_2 is doped with Zr, additional Zr^{4+} ions could be quartered into its matrix, thus changing its physical things (Reddy et al. 2017). The Zr^{4+} performance as a dual contributor provides up to binary further free electrons per ion replaced for Sn^{2+}, and therefore, it is invented that Zr doping could augment the optical and the photocatalytic stuff of SnO_2 actual much. Hence the extant work, a series of zirconium-doped SnO_2 (Zr:SnO_2) by different concentrations of Zr (2 and 4%) NPs were excellently blended by a modest proficient hydrothermal co-precipitation manner and the physical belongings remained deliberate and described. The Zr:SnO_2 NPs revealed highly improved photocatalytic possessions to methyl orange (MO) aqueous organic dye degradation. Meanwhile, the probable growth progression and photocatalytic mechanism were conversed to intricate the charge transfer alleyways of photoinduced charge carriers in a photocatalytic manner, individually. Likewise, the antibacterial activity was achieved in contradiction of *E. coli* and *S. aureus* microbes/bacteria by an agar well diffusion scheme to discover the aptness of Zr:SnO_2 NPs towards biological applications.

Experimental

Materials and reagents

Tin (IV) chloride pentahydrate ($SnCl_4{\cdot}5H_2O$), zirconium nitrate $Zr(NO_3)_4$, sodium hydroxide (NaOH), isopropanol (IPA), ethylene diamine tetra-acetic acid (EDTA), benzoquinone (BQ), and absolute ethanol (CH_3CH_2OH) were obtained from SDFCL Chemical Reagent Co., Pvt. Ltd., India, and used as customary without bonus modification. Deionized water (D.I) was used into entire synthesis progressions.

Sample preparation

The Zr:SnO_2 NPs with altered concentrations of Zr (2 and 4%) were organized by facile hydrothermal co-precipitation mode. The 0.1 M of $SnCl_4{\cdot}5H_2O$ was used as a precursor for organizing the SnO_2 NPs. The $SnCl_4{\cdot}5H_2O$ was dissolved in an HCl and D.I water mixture solution (1:4 with an overall of 50 mL). To this effect, NaOH solution (1 g NaOH was softened in 20 mL D.I water) was auxiliary by drops sage, under vital stirring to upswing the pH value as ~ 10. To realize Zr doping, Zr $(NO_3)_4$ (% of Sn source) attention was more auxiliary to the pioneer solution. The ensuing solution was well-stirred for 6 h and consequently progressed by Teflon-lined stainless-treated autoclave and preserved at 200 °C for 24 h. Thus, the white precipitate was conquered, and additional wash away for plentiful times by absolute ethanol and D.I water surveyed by drying at 60 °C. The consequent product was formerly crushed with an agate mortar to acquire (2 and 4%) Zr:SnO_2 NPs.

Characterization

The crystal structures of as-obtained samples remained examined on a powder XRD analysis were realized by X-ray diffractometer (Rigaku Miniflex II) through CuKα radiation ($\lambda = 1.5406$ Å) X-ray basis. The average crystallite size of the as-prepared samples is calculated from the Debye–Scherrer equation.

$$D = K\lambda/(\beta \cos\theta)$$

where K is the Scherrer constant (0.89), λ is the wavelength (X-ray), β is the full width of half-maximum, and θ is the diffraction angle. The surface morphologies were scrutinized by field emission scanning electron microscope (FESEM; HITACHI S-3000 H) enquiry. FTIR revisions were done by PerkinElmer RX-1 FTIR spectrophotometer. The optical belongings were categorized by a UV–Vis DRS spectrophotometer (JASCO UV–Vis–NIR V-770PC). Photoluminescence (PL) spectra fields were detailed using the JASCO FP8300 Spectrofluorometer at an excitation sequence of 292 nm. The photocatalytic presentations of the attained Zr:SnO_2 NPs were considered via the deprivation of MO aqueous dye (20 ppm; 10 mg/L) under treatment of a high-pressure mercury spotlight (300 W) done by 10 mg of structured samples as photocatalysts (PCs). Afterwards existence stirred in the dark area aimed at 30 min to conquer adsorption–desorption symmetry circumstance, and the mix was exposed to light irradiation. The absorptions of MO dye solution were reserved to evaluate the photocatalytic degradation efficacy at certain time intervals by a UV–Vis spectrophotometer (PerkinElmer Lambda-19). The trapping mechanism was carried out via IPA, BQ and EDTA in this effort remained used as the hydroxyl ($^{\cdot}OH$), superoxide radicals ($^{\cdot}O^{2-}$) and holes (h^+) scavengers, separately.

Assessment of antibacterial activity

The antibacterial studies of Zr-doped SnO_2 NPs were done by test organisms of *E. coli* (*Escherichia coli*; Gram − ve) and *S. aureus* (*Staphylococcus aureus*; Gram + ve) bacterial strains patterned via agar well diffusion way; similarly, the Muller Hinton agar was further used for bacteriological culture (Vignesh et al. 2019a). The plate organized for agar wells by hovering out the type with a hygienic tool

was overloaded with diverse attentiveness of 50 and 100 µL of obtaining pristine and Zr:SnO_2 solution; formerly, these cultures were positioned in the shaking incubator for 37 °C at 24 h for evolution. Likely, the negative control (dimethyl sulfoxide—DMSO) and positive control (ampicillin) ethics were restrained in the alike progression. When the cultivation period was done, the diameters of zone of inhibition ideals (ZOI) fashioned about the wells were inspected and noted. Both testings were finished in triplicate, and the ZOI are specified as the mean ± usual deviance.

Results and discussion

Structural characterization

The crystal structure and phase configurations of as-obtained pristine and Zr:SnO_2 (2% and 4%) NPs were classified and are publicized in Fig. 1. All the X-ray diversion points at $2\theta = 26.62°$, 33.88°, 37.98°, 51.8°, 54.84° and 57.86° consistent with the (110), (101), (111), (211), (220) and (002) planes, respectively, might be fine indexed for tetragonal rutile structure of SnO_2 (JCPDS 41-1445) (Yang et al. 2018), and nope apparent typical peaks of impurities are perceived (Fig. 1a). It directs the Zr dopants might be assimilated into the matrix of SnO_2 NSs. Moreover, the (110) and (101) diffraction peaks are supervised to probe the impact of doping on the crystal structure of SnO_2. Figure 1b unveils the X-ray diffusion points of the models were shifted to inferior angle, and the intensity was declined progressively by the doping attention, which proposes the doping of Zr results in the lattice distortion and authorizes the integration of Zr in Zr:SnO_2 NSs (Sujatha et al. 2019). The crystalline sizes of the pristine and Zr:SnO_2 NPs were considered by (FWHM) values with Scherrer's formula (Palanisamy et al. 2018), and the typical crystallite size is progressively reduced to 41.9, 38.97 and 35.85 nm for pristine, 2 and 4% Zr-doped SnO_2 NPs individually. The consequence was visibly designated that the grain growing of SnO_2 NPs was suppressed, owing to Zr, and it was substitutionary fixed with SnO_2 host lattice site (Babu et al. 2018).

Figure 2 illustrates the FTIR bands of pristine and Zr:SnO_2 NPs. The wide absorption stretching group in the range of 2700–3500 cm^{-1} was indorsed to the symmetric vibration of apparent hydroxyl (–OH) assembly (Bhuvaneswari et al. 2019). There are prospects of hints of atmospheric carbon-centred functionalization on the superficiality of Zr:SnO_2 NPs which might replicate amongst 1400–1800 cm^{-1} (Bhuvaneswari et al. 2018a).The absorption groups in the region 830–480 cm^{-1} could be consigned to many stretching manners connected with metal oxides (Azam et al. 2012). In this circumstance, the band could be qualified to the Sn–O groups in the Zr:SnO_2 NPs. The supreme apparent peaks were perceived at 503 cm^{-1}, agreeing to the Sn–O–Sn elongating mode (Li et al. 2008). However, nope peaks exact to Zr–O bands were patently signifying the doping of Zr into the SnO_2-structured matrix as detected in XRD extent.

Figure 3a, c indicates the surface morphological evolutions of as-attained bare SnO_2 and 4% of Zr:SnO_2 NSs using FESEM fallouts. The Zr:SnO_2 NPs yields were comprised of abundant consistent nanostructured agglomerated particles. In accumulation, the circulation of NPs with the superficial of SnO_2 NSs is clear. Conversely, there is a collecting phenomenon of nanostructures were expecting the structure feature was most constructive for the improvement

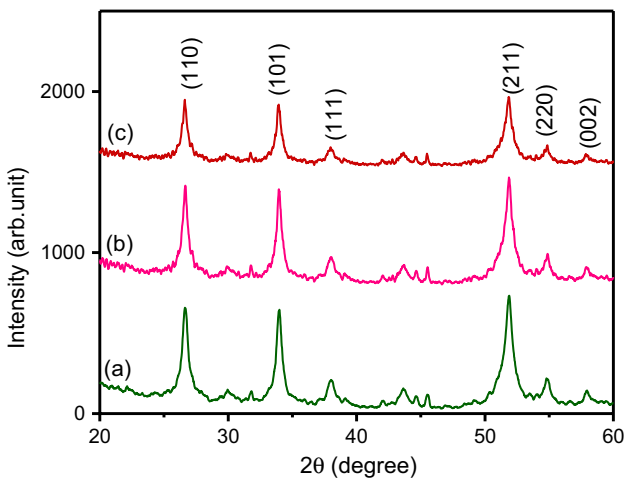

Fig. 1 XRD pattern of (a) SnO_2, (b) 2% Zr-doped SnO_2 NPs and (c) 4% Zr-doped SnO_2 NPs

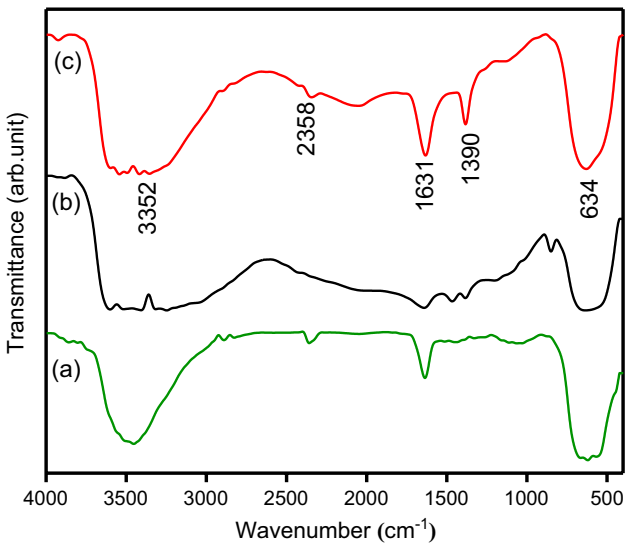

Fig. 2 FTIR spectra of (a) SnO_2, (b) 2% Zr-doped SnO_2 NPs and (c) 4% Zr-doped SnO_2 NPs

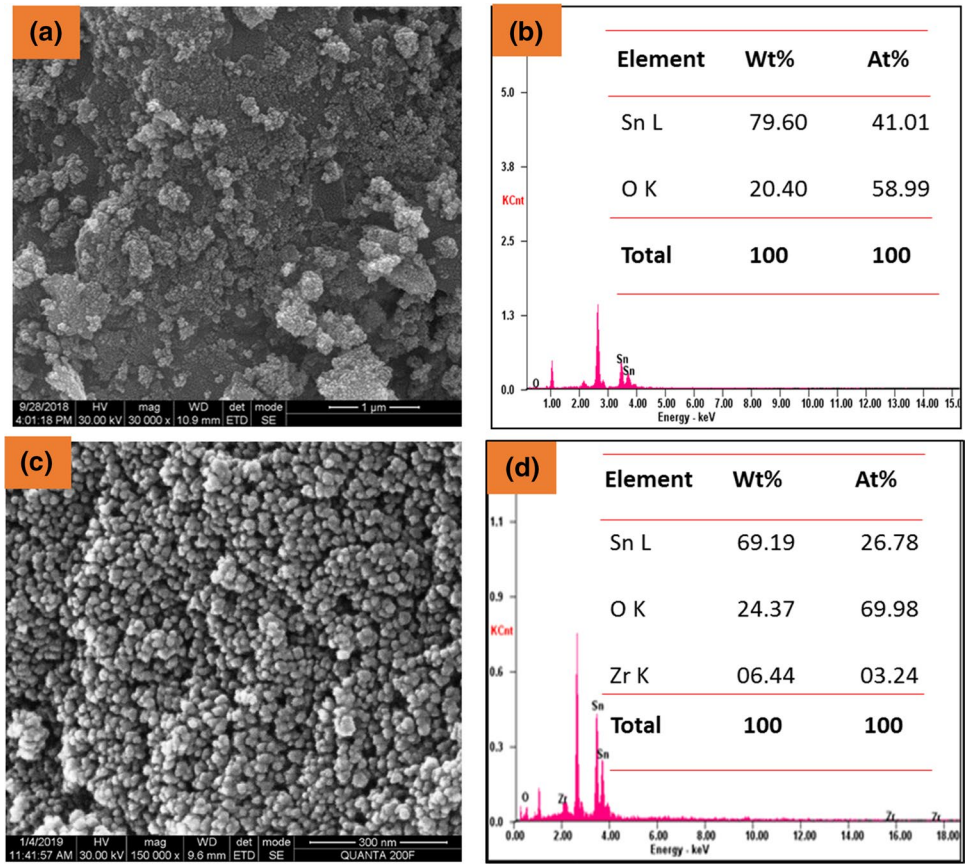

Fig. 3 **a**, **c** FESEM images and **b**, **d** EDAX spectra of SnO_2 and 4% Zr-doped SnO_2 NPs

of light adsorption capability of organic pollutants in the photocatalytic progression. Figure 3b, d spectacles the EDX spectrum of bare SnO_2 and 4% of Zr:SnO_2 NPs which leaks the incidence of (O and Sn) and (O, Sn and Zr) elements in the corresponding samples. Furtherly, no impurity peak was identified, hence it has recognized that Zr ions consume excellently imported the Sn in the SnO_2 lattice, which specifies the clearness of related composition. Even so, the uniform distribution nature was accessible in the essence of Sn, O and Zr species remained to establish since the EDX elemental mapping (Fig. 4) fallouts.

Optical properties of obtained NMs

It is recognized that the optical possessions of SCs nanomaterials are thoroughly interrelated to their photocatalytic presentation (Vignesh et al. 2018). The optical absorption assets of pristine and Zr:SnO_2 (2 and 4%) NPs were detailed with the UV–Vis DRS spectrum. Figure 5a indicates that the photoabsorption passion parades a sharp absorption/captivation edge at nearby 292 nm and henceforth solid growth in the UV to the visible region with the upsurge of the doping attentiveness. Likened with former samples, 4% of Zr:SnO_2 NPs has expressively boosted absorption in the visible region. The Tauc affiliation ($(\alpha h\nu)^2 = K(h\nu - E_g)^n$) was used to appraise the ethics of the bandgap energy (E_g) of the Zr:SnO_2 NPs (Palanisamy and Pazhanivel 2018). Here α stands for the optical absorption coefficient, h stands for Planck constant, ν stands for the photon frequency, K is virtually constant, and n is equivalent to 1/2 and 2 for direct/indirect certified transition (SnO_2) separately (Zhang et al. 2011). Thus, as shown in Fig. 5b, the E_g of the organized samples is assessed to be 3.49, 3.29 and 2.87 eV with the pristine, 2 and 4% of Zr:SnO_2 NPs, separately. Since the outcomes, the absorption edges of the Zr:SnO_2 NPs were pragmatic to shift faintly to the lower wavelength crosswise on increasing the attention Zr at 4%. Apparently, these redshifts and condensed bandgap caused from whichever the faults triggered by bit quantities of Zr^{4+} in the SnO_2 host lattice or the condensed crystal provinces. As a consequence, there is a decline in the operative bandgap and a swing in the band edges. Accordingly, by fluctuating the ratified size of the specified NPs, it is conceivable to improve the redox perspective of the conduction band (CB) electrons (e^-) and valence band (VB) holes (h^+). By the decreasing of the crystalline size, size-quantized NPs and the distribution of the photoexcited electrons/holes (e-/h+) since substance to fast surface changes, which might key to an increases of the photocatalytic effort.

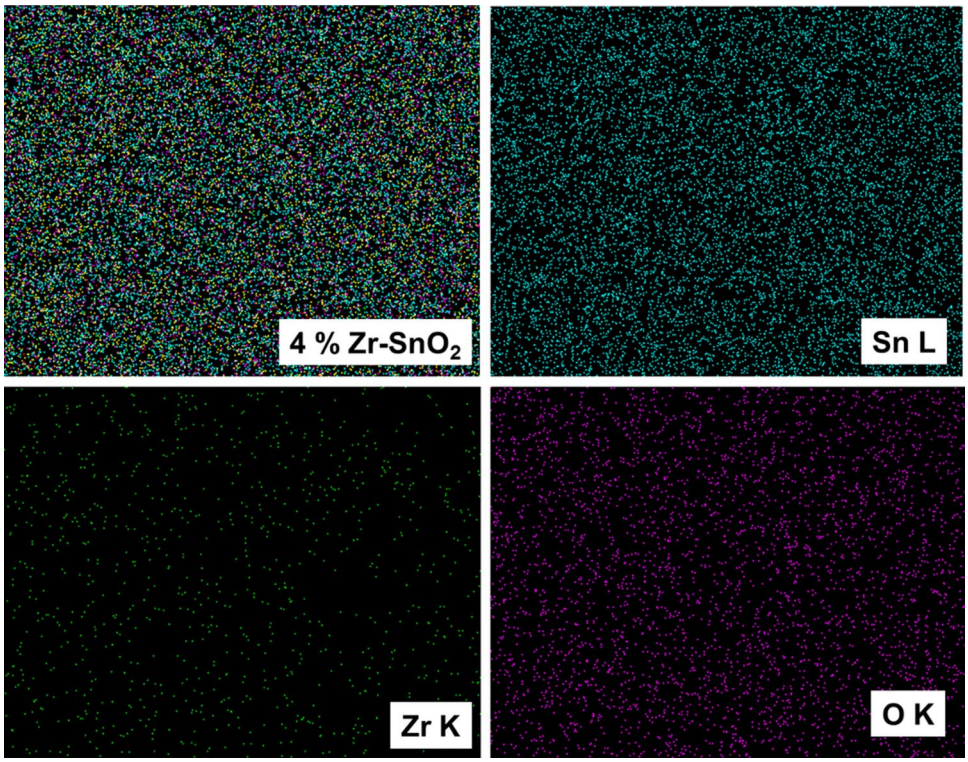

Fig. 4 EDAX elemental mapping of 4% Zr-doped SnO_2 NPs

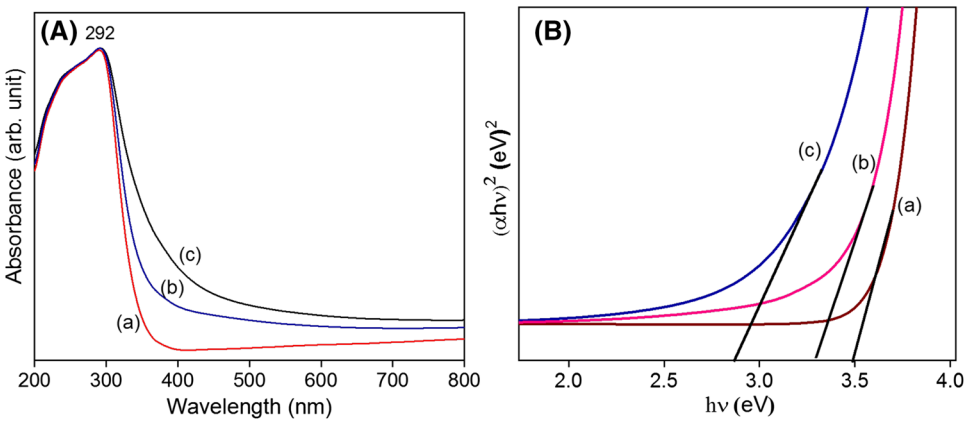

Fig. 5 **A** UV spectra and **B** bandgap energy of (a) SnO_2, (b) 2% Zr-doped SnO_2 NPs and (c) 4% Zr-doped SnO_2 NPs

Photoluminescence (PL) spectroscopy study supports to recognize the transfer conduct/recombination rate of the photoexcited (e^-/h^+) pairs (Zhou et al. 2015). Figure 6 shows the PL spectra of SnO_2 and doped Zr:SnO_2 NPs. This order of pristine and doped SnO_2, the PL spectrum confirms an broad and excessive concentrated visible emission positioned at around ~423 nm, which ascends owing to the realization of crystalline flaws through growth progression (Nehru et al. 2012). The existence of high densities being oxygen vacancy (V_o) or Sn interstitial customs a deficient level within the bandgap of SnO_2 NMs. The interface among these V_o or Sn interstitial makes an appropriate amount of limited positions constant energy levels, which outcomes in a prevailing PL emission, moreover to recombine the photoexcited charges (Kar et al. 2011). The 4% of Zr doping SnO_2 NPs indicates that the condensed PL intensity than pristine SnO_2 directs that active charge separation and the inhabitation rate of (e^-/h^+) recombination. The PL emission of the 4% of Zr-doped SnO_2 NPs was evidently authorized the vastly effectual separation of the photoexcited (e^-/h^+) pair (Bhuvaneswari et al. 2018b). At the time, Zr ions shows a key character in trapping the photoexcited electrons (e^-) from SnO_2 to create promising charge carriers separation, which was auxiliary authorized the enhanced visible-light photocatalytic performance of the Zr:SnO_2 NPs. Amid the results, Zr:SnO_2 NPs were

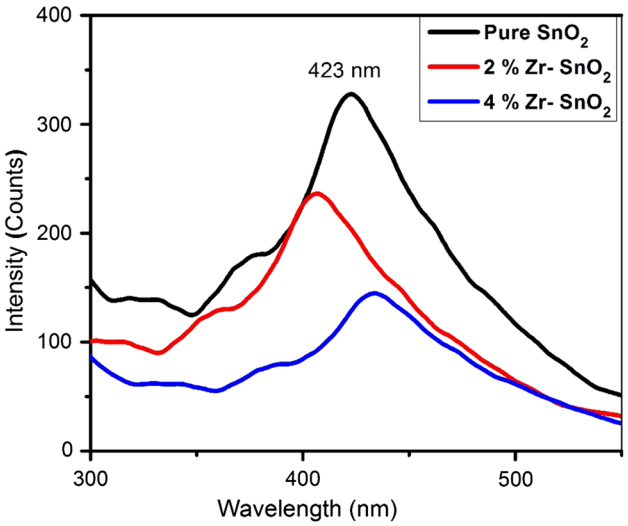

Fig. 6 PL spectra of SnO_2, 2% Zr-doped SnO_2 NPs and 4% Zr-doped SnO_2 NPs

actually assumed by augmented photocatalyst to expression for superior photocatalytic action.

Photocatalytic activity measurements

MO is one of the typical pollutants (generally used dye) and has been broadly used to appraise the photocatalytic presentation of achieved PCs. As-obtained pristine and Zr-doped SnO_2 NPs were approved as catalysts, and the photocatalytic degradation assessments towards MO aqueous dye were passed out. Figure 7a shows the progress of UV–Vis absorption spectra of MO dye spectral deviations through the photocatalytic progression of 4% Zr:SnO_2 NPs. Likewise Fig. 8 provides the photodegradation rates (C/C_0) of MO dye in existence of as-obtained catalysts under visible-light revelation. The degradation efficacy of pristine SnO_2 NPs is 34.4% after 180 min of visible-light revelation. Remarkably, 89.6% of MO dye was decayed with the actuality of 4% Zr:SnO_2 NPs under the identical conditions for 180 min, although the 2% Zr:SnO_2 NPs expose that 74.4% degradation at the

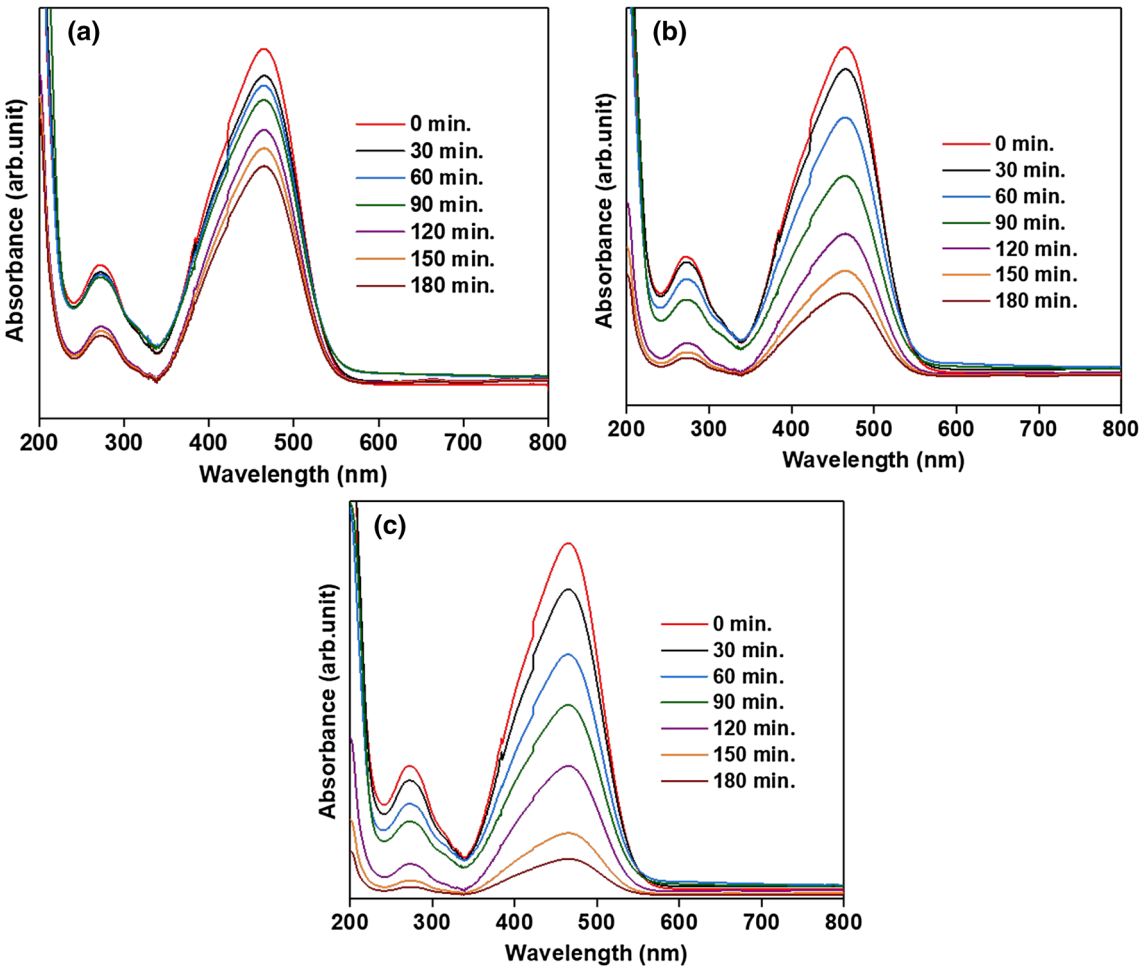

Fig. 7 UV–visible absorption spectra of MO degradation of samples **a** SnO_2, **b** 2% Zr-doped SnO_2 NPs and **c** 4% Zr-doped SnO_2 NPs

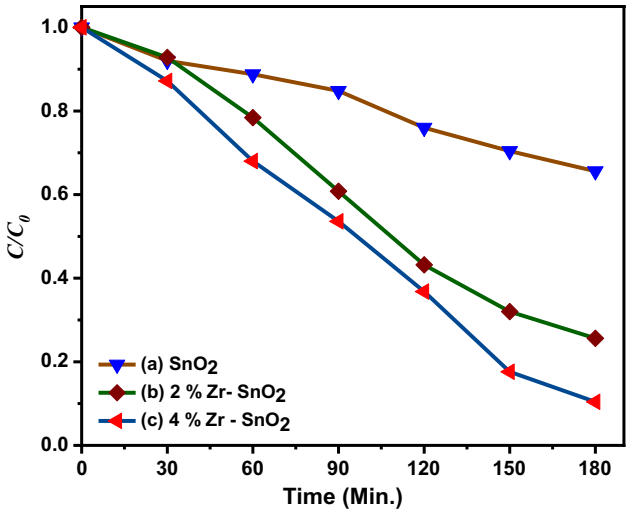

Fig. 8 Photocatalytic degradation of MO (a) SnO_2, (b) 2% Zr-doped SnO_2 NPs and (c) 4% Zr-doped SnO_2 NPs

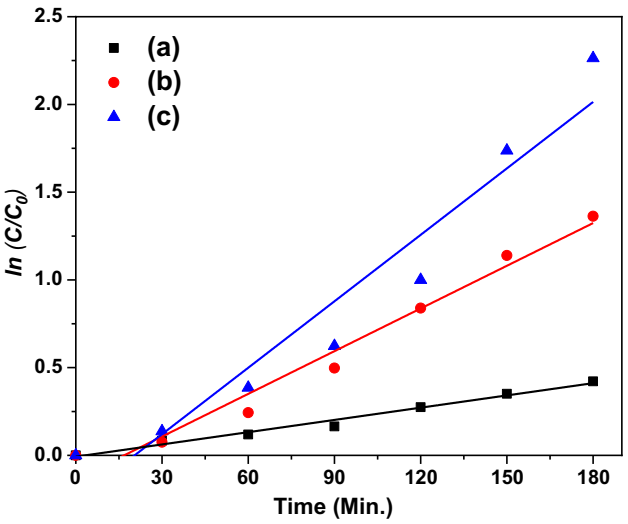

Fig. 10 First-order kinetic plot for the degradation of MO over (a) SnO_2, (b) 2% Zr-doped SnO_2 NPs and (c) 4% Zr-doped SnO_2 NPs

matching time and exposure, separately. Hence, 4% dopant of Zr:SnO_2 photocatalyst presence for an improved photocatalytic performance in compared with the pristine SnO_2 PCs. Figure 9 indicates the degradation rates for the greater photocatalytic presentation of the 4% Zr:SnO_2 PCs with the upsurges of the Zr doping attention. In accumulation, the blank trial was used as a disparity with photodegradation rate was also verified. To well explore the photocatalytic possessions of obtained samples, the responsive kinetic performance was scrutinized. The MO dye photodegradation rates were tailored by the pseudo-first-order kinetic association (kinetics model; $\ln(C/C_0) = kt$) plots as clarified in Fig. 10, where k stands for the rate constant, and C_0 and C are the primary attentiveness and time t, separately. The

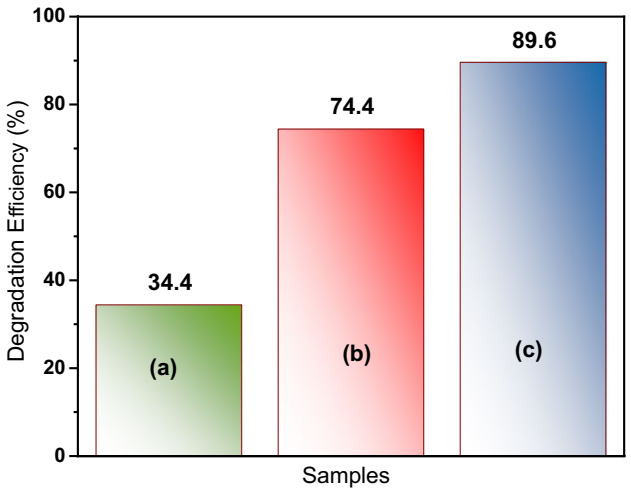

Fig. 9 Degradation efficiency of MO (a) SnO_2, (b) 2% Zr-doped SnO_2 NPs and (c) 4% Zr-doped SnO_2 NPs

pristine and Zr:SnO_2 (2 and 4%) NPs indicate upright linear affiliation too deviations amongst $\ln(C/C_0)$ versus time (t). The consistent reactive rate constants (k) are exposed in Fig. 10, and the obtained ideals are 0.00233, 0.00811 and 0.01262 min^{-1} for pristine, 2 and 4% of Zr:SnO_2 NPs, separately. Exactly, the value of k by 4% of Zr:SnO_2 PCs was around 5.41 times as high as that of the pristine SnO_2. Furthermore, this effort has heightened photocatalytic presentation of the doped NMs which might essentially be recognized to the occurrence of the oxygen vacancies (V_o) and Zr hubs. Instead, the oxygen vacancies (V_o) and Zr interiors could publicize in-between deficiency energy positions in the bandgap and reduction of the excitation energy (Ahmed 2010).

Additionally, the prevailing oxygen vacancies (V_o) and incapacitating Zr^{4+} centres could act as arrested hubs for photoexcited charge carriers/(e^-/h^+), however supportive to diminish the recombination evolution of the particulars. Similarly the remarkable doping considerations (6% of Zr) and crystallite sizes are favorable for the larger photocatalytic performances.

To authenticate the steadiness and reusability of 4% of Zr:SnO_2 PCs were further used four times under visible-light exposure, as presented in Fig. 11. Since Fig. 11, the recycling method, after four sequential cycling turns of the MO colourant (20 ppm) photodegradation for the identical conditions. The degradation activity of the 6% Zr: SnO_2 PCs presences a minor degeneration likewise minor loss of activity after four cycles due to the loss of the PCs through the washing in between the recycling process. Accordingly, the 4% Zr:SnO_2 photocatalyst remained relatively steady and has considerable potential application in wastewater handling. These causes for this heightening of activity were owing

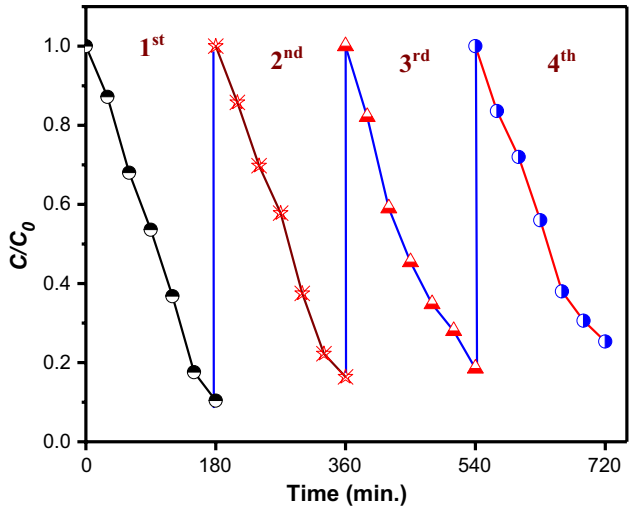

Fig. 11 Four repeated processes of 4% Zr-doped SnO_2 NPs for photodegradation of MO under UV–visible-light irradiation

to the synergistic outcome of the fitting Zr content, which transferences the photoexcited electrons (e^-) since the CB of SnO_2. The catalyst as well exposed under the XRD pattern and FTIR descriptions after four consecutive catalytic cycles, and there is no modification in the structural diffraction peaks and crucial functional groups of the catalyst correlated with that of earlier photocatalysis as shown in Fig. 12a, b separately.

To explore the pathway of photocatalytic evolution in the MO dye deprivation progression through 4% of Zr:SnO_2 photocatalyst, the trapping tests of diverse reactive species were done. In Fig. 13, the scavengers illustrate varied impressions scheduled the photocatalytic degradation rate heritages. However, with the addition of (0.5 mM) IPA, and (1 mM) BQ was an extensive decrease on the degradation rate arises, which designating that hydroxyl (.OH) and superoxide radicals ($\cdot O^{2-}$) as a scavengers are the vital active species and performs strategic characters in the photocatalytic progression of MO dye under visible-light region. Similarly, when EDTA (1 mM) was familiarized, the deprivation rate declines somewhat, signifying h^+ plays a trivial part in the MO dye deprivation manner.

Photocatalytic mechanisms of obtained photocatalyst

The credible photocatalytic appliance of photoexcited charge carriers, immigration of 4% of Zr:SnO_2 photocatalyst for deprivation of organic MO dyes and graphical electronic construction for strangely enlightening the photocatalytic recital are explained in Fig. 14. By the visible-light excitation, the photoexcited electrons could jump from VB to CB and authority of holes (h^+) on the VB at the equal time period. Related to pristine SnO_2, the 4% of Zr:SnO_2 NPs shows the lesser bandgap and the sturdier light absorption; thus, further charge carriers could be motivated by the progression and then contributed to subsequent photocatalytic responses. As 4% of Zr:SnO_2 PCs own V_o and Zr hubs, certain photoexcited (e^-) could openly transference to the CB, although the respite could be arrested by the dopant of Zr interiors and deficiency energy involvement prompted by (V_o) under the CB adjacent (Ahmed 2010; Palanisamy et al. 2018). It is obliged to gentle down the recombination and persists the lifetime of photoexcited charges. Meanwhile, the

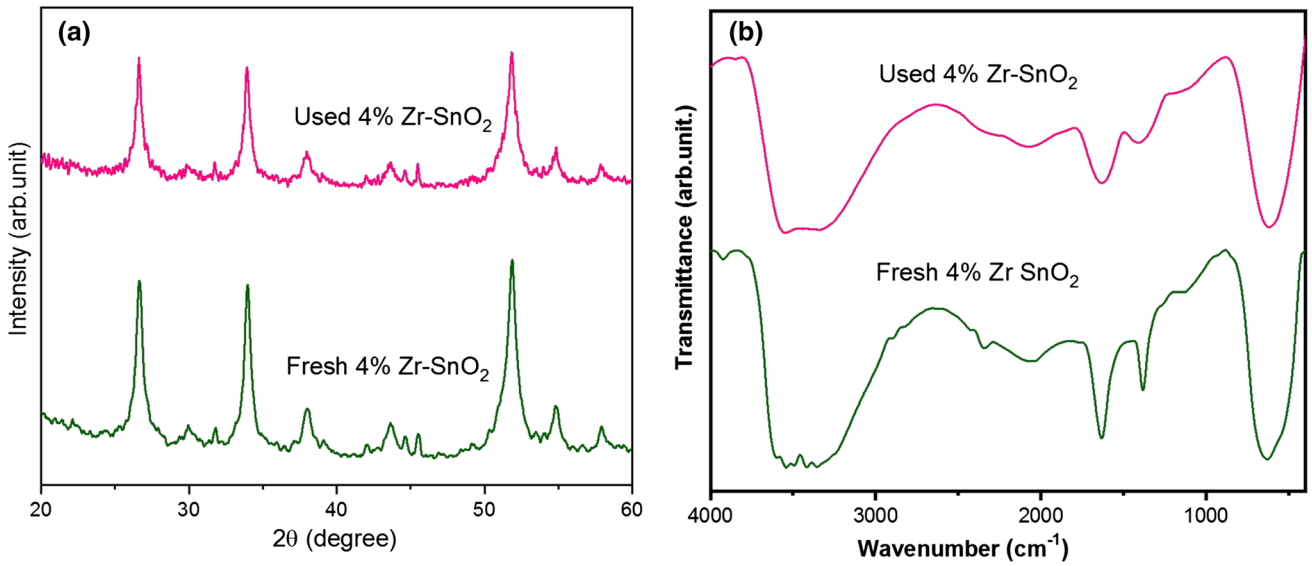

Fig. 12 XRD pattern and FTIR spectra for 4% Zr-doped SnO_2 NPs fresh and used photocatalytic reaction

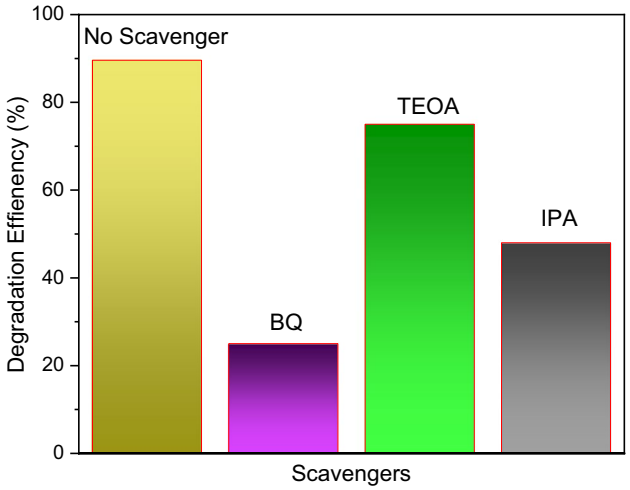

Fig. 13 Effects of different scavengers on the degradation of MO dye in the presence of 4% Zr-doped SnO_2 NPs

(V_o) circulated on shallow might stimulate the O_2 adsorption, and it could quicken the creation of $.O^{2-}$ extremists which are attested to be one of the foremost reactive species. Likewise, the 4% Zr:SnO_2 PCs has further photoactivity activity could be provided with visible-light harvest and degraded the dye molecules. Under the light irradiation, ($.O^{2-}$) radicals could be fashioned over the trapping of photoexcited electrons (e^-) via softened oxygen molecules, whereas photoexcited holes (h^+) could respond to producing the H_2O and hydroxyl (.OH). As fashioned, ($^{\cdot}OH$) and ($^{\cdot}O^{2-}$) are robust oxidizing mediators and could contribute to the deprivation of MO dye grains. These photoexcited (e^-) are rapidly transported to SnO_2. The conveyed (e^-) at SnO_2 surface is hunted by softened oxygen molecules in the water moderate to custom superoxide radical anions ($.O^{2-}$) and (.OH) hydroxyl radicals. Additionally, the (h^+) on the Zr superficial is confined through OH to form $.OH^-$ species that were specifically aimed at the oxidation of dye contaminant (Vignesh et al. 2019b). Supportive to the graphic outline for the photocatalytic activity of the proposed manner by Zr:SnO_2 PCs of surface behavior in the photoexcited electrons (e^-) as anticipated for photodegradation of MO dye as monitored: Eqs. (1–3).

$$\text{Zr:SnO}_2\text{NPs} + \text{Dye} + \text{Visible light} \rightarrow \text{Zr:SnO}_2 + \text{Dye} + \left(e^-(\text{CB}) + h^+(\text{VB})\right) \quad (1)$$

$$\text{MB Dye molecule} + \text{OH} \rightarrow \text{OH}^{\cdot -} + \text{Degradation Products} \quad (2)$$

$$\text{MB Dye molecule} + \text{O}_2 \rightarrow \text{O}_2^{\cdot -} + \text{Degradation Products} \quad (3)$$

Thus, the photocatalytic recital of 4% Zr:SnO_2 nanostructured PCs is intensely upgraded owing to the synergistic things, which embrace the sturdier light fascination, the calmer light excitation, the improved charge carrier's departure, further effectual of oxygen adsorption and additional photoactivity sites. In addition, the photocatalytic presentations of the as-obtained 4% of Zr:SnO_2 PCs were associated with recently testified PCs by different semiconductors metal

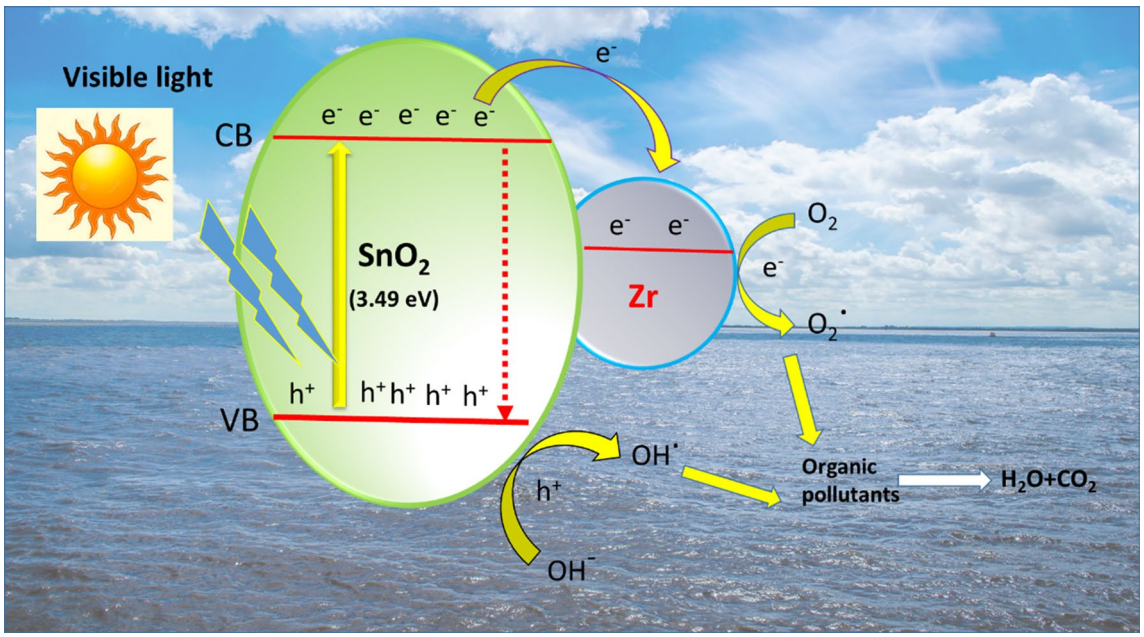

Fig. 14 The plausible mechanism of the MO dye degradation for 4% Zr-doped SnO_2 NPs

Table 1 Comparison of visible-light generated MO degradation rate (%) over previously reported nanomaterials

S. no.	Photocatalyst	Dye	Irradiation time (min)	Degradation efficiency (%)	References
1	Polyethersulfone–ZnO nanocomposite	MO	540	~ 98.82	Hir et al. (2017)
2	Carbon-coated alumina Ni-doped titanium dioxide NPs	MO	180	~ 81	Mbuli et al. (2019)
3	Mn–C–codoped TiO_2 nanoparticles	MO	300	~ 53	Xin et al. (2012)
4	Mg-doped TiO_2 polyscales	MO	300	~ 79	Shivaraju et al. (2017)
5	TiO_2/ZnO/GO nanocomposite	MO	170	~ 57.7	Raliya et al. (2017)
6	4% Zr-doped SnO_2 NPs	MO	180	~ 89.6	This work

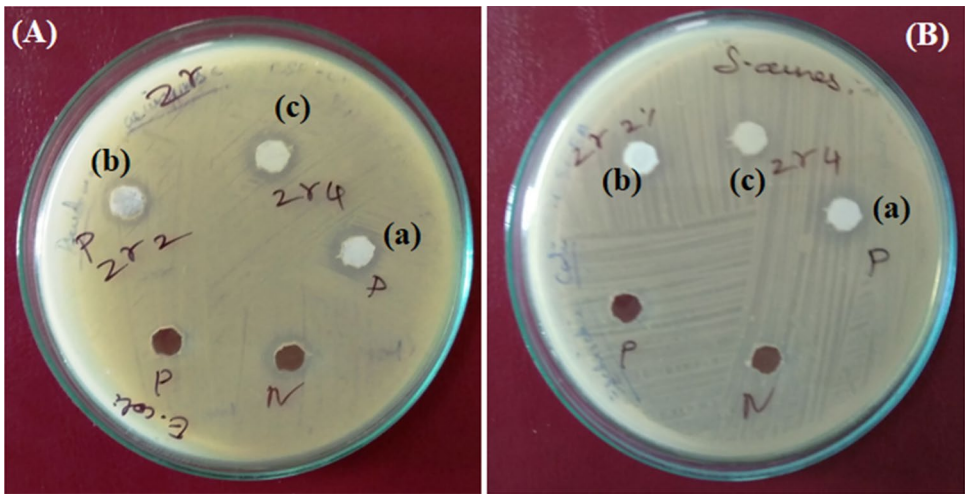

Fig. 15 Zone inhibition test for a SnO_2, b 2% Zr-doped SnO_2 NPs and c 4% Zr-doped SnO_2 NPs towards **A** *E. coli* and **B** *S. aureus* bacteria's

oxides/metal and auxiliary nanocomposites are deliberated in Table 1 (Xin et al. 2012; Shivaraju et al. 2017; Raliya et al. 2017; Hir et al. 2017; Mbuli et al. 2019). Hereafter it has comprehended that the Zr:SnO_2 PCs have upgraded catalytic proficiency analogized with further comprehensive photocatalytic materials.

The antibacterial actions of the Zr-doped SnO_2 NPs were verified via agar well diffusion method against *E. coli* and *S. aureus*. The antibacterial effectiveness was scrutinized from the ZOI established around the sample areas. Figure 15A, B displays the pictures of ZOI established around the obtained samples, and reliable values are charted in Table 2. All the Zr-doped SnO_2 NPs illustrate improved bacteriological retardant performance equated to the pristine sample besides the experienced pathogenic microbes. The inadequate antibacterial movement detected for the pristine SnO_2 NPs might be owing to its short diffusivity which inhibits the interface amongst the nanomaterials and microbial kinds (Chandran et al. 2015). The heightened antibacterial efficacy detected for the 4% of Zr:SnO_2 NPs might be owed to the contact amid their amended shells and microbes owing to adsorption–desorption and also chemical/physical capabilities. Owing to the enriched gathering of 4% of Zr:SnO_2 NPs on the superficial of the microbes/bacteria, the cytoplasmic

Table 2 Assessment on zone of inhibition of antibacterial activity for as-prepared nanoparticles

S. no.	Microorganisms	Zone of inhibition range (mm)	
		E. Coli.	*S. aureus*
1	SnO_2	4 ± 0.5	3 ± 1
2	2% Zr-doped SnO_2 NPs	5 ± 1	3 ± 0.5
3	4% Zr-doped SnO_2 NPs	7 ± 0.5	5 ± 0.5

phospholipid cell membrane interruption takes place triggering the cell death (Shanmugam and Jeyaperumal 2018). It has fine identified that reactive/regenerative oxygen species (ROS) are being fashioned once the NPs enter into the cell barrier of microbes owing to their surface response on the cell wall exterior. The ROS kinetics hydrogen peroxide (H_2O_2), superoxide radical anions (.O^{2-}), (.OH) hydroxyl radicals and organic hydroperoxides source react with cell damage owing to the oxidative strain on the wall of the cell membrane (Shanmugam et al. 2018). The augmented steadiness and diminished crystallite size might furthermore be the potential object for the improved antibacterial action of the Zr:SnO_2 NPs (Amininezhad et al. 2015), and the NPs

incline to captivate on the bacterial surface and dehydrogenation owing to inhalation progression arises at the bacterial cell wall. The Zr^{4+}, a great valence metal ion-doped into hot SnO_2 matrix, might produce Sn vacancy (V_{Sn}) or oxygen interstitial by means to preserve the electric impartial stability prominent to the eccentricity of Sn/O proportion since their stoichiometry. Henceforth, the superior antibacterial activity was attained against *E. coli* and *S. aureus* bacteria, and also the Zr:SnO_2 NPs were suitable for pharmaceutical trick and biological applications.

Summary and conclusions

In summary, the 4% Zr:SnO_2 nanoparticles (NPs) were effectively produced by a modest and cost-efficient hydrothermal co-precipitation procedure. The XRD outcomes propose that nanocrystalline pristine and Zr-doped SnO_2 NPs by tetragonal rutile-type construction and the crystallite size are about ~ 41 to 36 nm. FESEM imageries expose that the 4% of Zr:SnO_2 NPs were self-possessed nanostructured with the agglomerated distribution of NPs and the EDX elemental enquiry endorses the manifestation of Zr metals was unvaryingly circulated over the SnO_2 outward. The optical bandgap values are considered as 3.49 eV and 2.87 eV for pristine and Zr-doped SnO_2 NPs separately. PL spectra fallouts advised that Zr dopant familiarized novel impurity planes amongst the CB and VB of SnO_2, prominent to slighter bandgap augmenting the visible-light fascination. The 4% of Zr-doped SnO_2 PCs influenced and enhanced photocatalytic activity and the superior deprivation efficacy towards MO dye under visible light. The deprivation rate of MO dye through Zr:SnO_2 was augmented from 34.4 to 89.6% in 180 min and hence 2.6 times greater than the association with the pristine SnO_2 NPs. The recycling test was established that through 4% Zr–SnO_2 catalyst has no reduction of catalytic activity in the four sequential series runs. This effect advises that Zr-doped SnO_2 catalyst might have prospective for good bacterial links and high concert visible-light-driven photocatalyst for the applications of industrial wastewater remediation.

Compliance with ethical standards

Conflict of interest The authors declare no conflict of interest in presenting this article.

References

Ahmed SA (2010) Room-temperature ferromagnetism in pure and Mn doped SnO_2 powders. Solid State Commun 150:2190–2193. https://doi.org/10.1016/j.ssc.2010.08.029

Amininezhad SM, Rezvani A, Amouheidari M et al (2015) The antibacterial activity of SnO_2 nanoparticles against *Escherichia coli* and *Staphylococcus aureus*. Zahedan J Res Med Sci. https://doi.org/10.17795/zjrms-1053

Arnold MS, Avouris P, Pan ZW, Wang ZL (2003) Field-effect transistors based on single semiconducting oxide nanobelts. J Phys Chem B 107:659–663. https://doi.org/10.1021/jp0271054

Azam A, Ahmed AS, Habib SS, Naqvi AH (2012) Effect of Mn doping on the structural and optical properties of SnO_2 nanoparticles. J Alloys Compd 523:83–87. https://doi.org/10.1016/j.jallcom.2012.01.072

Babu B, Kadam AN, Rao GT et al (2018) Enhancement of visible-light-driven photoresponse of Mn-doped SnO_2 quantum dots obtained by rapid and energy efficient synthesis. J Lumin 195:283–289. https://doi.org/10.1016/j.jlumin.2017.11.040

Bhuvaneswari K, Bharathi RD, Pazhanivel T (2018a) Silk fibroin linked Zn/Cd-doped SnO_2 nanoparticles to purify the organically polluted water. Mater Res Express 5:24004. https://doi.org/10.1088/2053-1591/aaaa35

Bhuvaneswari K, Palanisamy G, Pazhanivel T et al (2018b) Photocatalytic performance on visible light induced ZnS QDs-MgAl layered double hydroxides hybrids for methylene blue dye degradation. ChemistrySelect 3:13419–13426. https://doi.org/10.1002/slct.201803183

Bhuvaneswari K, Palanisamy G, Pazhanivel T et al (2019) Photodegradation activity of nitrogen-rich graphitic carbon nitride intercalated ZnO\Mg–Al layered double hydroxide ternary nanocomposites on methylene blue dye. ChemistrySelect 4:2982–2990. https://doi.org/10.1002/slct.201900146

Chandran D, Nair LS, Balachandran S et al (2015) Structural, optical, photocatalytic, and antimicrobial activities of cobalt-doped tin oxide nanoparticles. J Sol Gel Sci Technol 76:582–591. https://doi.org/10.1007/s10971-015-3808-z

Chen P, Mao Y, Hou S et al (2019) Growth of SnO_2 nanocrystals co-doped with Eu^{3+} for highly enhanced photoluminescence in mesoporous silica glasses. J Mater Chem C 7:1568–1574. https://doi.org/10.1039/c8tc04457k

Fu X, Li GG, Villarreal E, Wang H (2019) Hot carriers in action: multimodal photocatalysis on Au@SnO_2 core–shell nanoparticles. Nanoscale 11:7324–7334. https://doi.org/10.1039/c9nr02130b

Hendry E, Koeberg M, O'Regan B, Bonn M (2006) Local field effects on electron transport in nanostructured TiO_2 revealed by terahertz spectroscopy. Nano Lett 6:755–759. https://doi.org/10.1021/nl0600225

Hir ZAM, Abdullah AH, Zainal Z, Lim HN (2017) Photoactive hybrid film photocatalyst of polyethersulfone–ZnO for the degradation of methyl orange dye: kinetic study and operational parameters. Catalysts 7:313. https://doi.org/10.3390/catal7110313

Hu L, Zhang R, Chen Q (2014) Synthesis and assembly of nanomaterials under magnetic fields. Nanoscale 6:14064–14105. https://doi.org/10.1039/c4nr05108d

Kar A, Kundu S, Patra A (2011) Surface defect-related luminescence properties of SnO_2 nanorods and nanoparticles. J Phys Chem C 115:118–124. https://doi.org/10.1021/jp110313b

Li Z, Shen W, Zhang X et al (2008) Controllable growth of SnO_2 nanoparticles by citric acid assisted hydrothermal process. Colloids Surf A Physicochem Eng Asp 327:17–20. https://doi.org/10.1016/j.colsurfa.2008.05.043

Manjula N, Selvan G (2017) Magnetic and antibacterial properties of Zr-doped SnO_2 nanopowders. J Mater Sci Mater Electron 28:15056–15064. https://doi.org/10.1007/s10854-017-7380-x

Mbuli BS, Mahlambi MM, Ngila CJ, Moutloali RM (2019) Polysulfone ultrafiltration membranes modified with carbon-coated alumina supported Ni-TiO_2 nanoparticles for water treatment: synthesis, characterization and application. J Membr Sci Res 5:222–232. https://doi.org/10.22079/JMSR.2018.80046.1173

Nehru LC, Swaminathan V, Sanjeeviraja C (2012) Photoluminescence studies on nanocrystalline tin oxide powder for optoelectronic devices. Am J Mater Sci 2:6–10. https://doi.org/10.5923/j.materials.20120202.02

Palanisamy G, Pazhanivel T (2018) Investigation on the photophysical properties of tungsten trioxide and tungstate based nanocomposites. Mater Res Express 5:44001. https://doi.org/10.1088/2053-1591/aab735

Palanisamy G, Bhuvaneswari K, Bharathi G et al (2018) Enhanced photocatalytic properties of ZnS–WO_3 nanosheet hybrid under visible light irradiation. ChemistrySelect 3:9422–9430. https://doi.org/10.1002/slct.201801688

Raliya R, Avery C, Chakrabarti S, Biswas P (2017) Photocatalytic degradation of methyl orange dye by pristine titanium dioxide, zinc oxide, and graphene oxide nanostructures and their composites under visible light irradiation. Appl Nanosci 7:253–259. https://doi.org/10.1007/s13204-017-0565-z

Reddy NNK, Akkera HS, Sekhar MC, Park SH (2017) Zr-doped SnO_2 thin films synthesized by spray pyrolysis technique for barrier layers in solar cells. Appl Phys A Mater Sci Process 123:761. https://doi.org/10.1007/s00339-017-1391-6

Shanmugam V, Jeyaperumal KS (2018) Investigations of visible light driven Sn and Cu doped ZnO hybrid nanoparticles for photocatalytic performance and antibacterial activity. Appl Surf Sci 449:617–630. https://doi.org/10.1016/j.apsusc.2017.11.167

Shanmugam V, Muppudathi AL, Jayavel S, Jeyaperumal KS (2018) Construction of high efficient g-C_3N_4 nanosheets combined with Bi_2MoO_6–Ag photocatalysts for visible-light-driven photocatalytic activity and inactivation of bacterias. Arab J Chem. https://doi.org/10.1016/j.arabjc.2018.05.009

Shivaraju HP, Midhun G, Anil Kumar KM et al (2017) Degradation of selected industrial dyes using Mg-doped TiO_2 polyscales under natural sun light as an alternative driving energy. Appl Water Sci 7:3937–3948. https://doi.org/10.1007/s13201-017-0546-0

Song JS, Cho GB, Kim KW et al (2019) Fabrication of multilayer graphene-encapsulated Sn/SnO_2 nanocomposite as an anode material for lithium-ion batteries and its electrochemical properties. Appl Surf Sci 481:736–740. https://doi.org/10.1016/j.apsusc.2019.03.132

Sujatha K, Seethalakshmi T, Sudha AP, Shanmugasundaram OL (2019) Photocatalytic activity of pure, Zn doped and surfactants assisted Zn doped SnO_2 nanoparticles for degradation of cationic dye. Nano-Struct Nano-Objects 18:100305. https://doi.org/10.1016/j.nanoso.2019.100305

Vignesh K, Hariharan R, Rajarajan M, Suganthi A (2013) Photocatalytic performance of Ag doped SnO_2 nanoparticles modified with curcumin. Solid State Sci 21:91–99. https://doi.org/10.1016/j.solidstatesciences.2013.04.017

Vignesh S, Muppudathi AL, Sundar JK (2018) Multifunctional performance of gC_3N_4–$BiFeO_3$–Cu_2O hybrid nanocomposites for magnetic separable photocatalytic and antibacterial activity. J Mater Sci Mater Electron 29:10784–10801. https://doi.org/10.1007/s10854-018-9144-7

Vignesh S, Suganthi S, Kalyana Sundar J et al (2019a) Highly efficient visible light photocatalytic and antibacterial performance of PVP capped Cd:Ag:ZnO photocatalyst nanocomposites. Appl Surf Sci 479:914–929. https://doi.org/10.1016/j.apsusc.2019.02.064

Vignesh S, Suganthi S, Kalyana Sundar J, Raj V (2019b) Construction of α-Fe_2O_3/CeO_2 decorated g-C_3N_4 nanosheets for magnetically separable efficient photocatalytic performance under visible light exposure and bacterial disinfection. Appl Surf Sci 488:763–777. https://doi.org/10.1016/j.apsusc.2019.05.147

Xin W, Zhu D, Liu G et al (2012) Synthesis and characterization of Mn–C–codoped TiO_2 nanoparticles and photocatalytic degradation of methyl orange dye under sunlight irradiation. Int J Photoenergy. https://doi.org/10.1155/2012/767905

Yang T, Zhu M, Gu K et al (2018) Facile synthesis of SnO_2 nanoparticles for improved formaldehyde detection. New J Chem 42:13612–13618. https://doi.org/10.1039/c8nj01923a

Zhang J, Wang Y, Li S et al (2011) Controlled synthesis, growth mechanism and optical properties of $FeWO_4$ hierarchical microstructures. CrystEngComm 13:5744–5750. https://doi.org/10.1039/c1ce05416c

Zhou B, Xiong X, Yang S et al (2015) In situ construction of an SnO_2/g-C_3N_4 heterojunction for enhanced visible-light photocatalytic activity. RSC Adv 5:68953–68963. https://doi.org/10.1039/c5ra11801h